*Atmos. Sci. Let.* **16**: 77–82 (2015)
Published online 25 August 2014 in Wiley Online Library (wileyonlinelibrary.com) **DOI:** 10.1002/asl2.524

RMetS Royal Meteorological Society

# Towards an aerosol classification scheme for future EarthCARE lidar observations and implications for research needs

S. Groß,[1]* V. Freudenthaler,[2] M. Wirth[1] and B. Weinzierl[1,2]

[1]*Institut für Physik der Atmosphäre, Deutsches Zentrum für Luft- und Raumfahrt (DLR), 82234 Oberpfaffenhofen, Germany*
[2]*Meteorologisches Institut, Ludwig-Maximilians-Universität, 80333 Munich, Germany*

**Correspondence to:*
*S. Groß, Institut für Physik der Atmosphäre, Deutsches Zentrum für Luft- und Raumfahrt (DLR), 82234 Oberpfaffenhofen, Germany.*
*E-mail: Silke.Gross@dlr.de*

Received: 28 August 2013
Revised: 8 April 2014
Accepted: 21 July 2014

## Abstract

**Owing to the high variability of aerosols, and their different impact on the Earth's climate system, aerosol type classification from satellite measurements is of high importance. Polarization sensitive lidar measurements on board the future Earth Clouds, Aerosols and Radiation Explorer (EarthCARE) satellite mission will provide information to distinguish different aerosol types. We analyze whether former classification schemes based on lidar measurements at 532 nm are applicable to EarthCARE measurements at 355 nm. We compare coordinated lidar measurements at both wavelengths performed during five field experiments; adapt thresholds for aerosol classification with future spaceborne lidar measurements and identify limitations of the current state of knowledge.**

**Keywords:** **aerosols; EarthCARE; lidar; remote sensing; classification**

## 1. Introduction

Aerosols are a fundamental part of the Earth's atmosphere with various impacts on the Earth's radiation budget and hydrological cycle. These numerous effects are not yet fully understood (Forster *et al.*, 2007; Penner *et al.*, 2011; Bond *et al.*, 2013). A main reason is the large variability and the limited knowledge of the temporal and spatial distribution of the optical and microphysical properties of aerosols on global scales (Penner *et al.*, 2001). In addition the sign and the magnitude of the radiative forcing strongly depend on the vertical layering of aerosols and the presence of clouds underneath the aerosol layers (Forster *et al.*, 2007). To improve our understanding regular observations with high vertical and horizontal resolution are required. Spaceborne measurements with elastic backscatter lidar systems such as the Cloud-Aerosol Lidar with Orthogonal Polarization (CALIOP) system (Winker *et al.*, 2007) on board the Cloud-Aerosol Lidar and Pathfinder Satellite Observations (CALIPSO) mission gather such altitude-resolved information. However, for the classification of different aerosol types assumptions are necessary (Omar *et al.*, 2009) which may cause misclassification (Kacenelenbogen *et al.*, 2011; Burton *et al.*, 2013). Advanced lidar systems like polarization sensitive Raman lidar systems (Ansmann *et al.*, 1992) or high spectral resolution lidar (HSRL) systems (Piironen and Eloranta, 1994; Esselborn *et al.*, 2008) are capable of distinguishing different aerosol types as shown, e.g. by Groß *et al.* (2011a, 2013b), Weinzierl *et al.* (2011), and Burton *et al.* (2012), as they are capable of directly retrieving the lidar ratio without assumptions of a priori information. At the moment, these lidar systems are either airborne or ground-based, but the next generation satellite mission of the European Space Agency (ESA) together with the Japan Aerospace Exploration Agency (JAXA), the Earth Clouds, Aerosols and Radiation Explorer (EarthCARE) mission will be equipped with a polarization sensitive HSRL system (ATLID – Atmospheric Lidar) operating at 355 nm. Current aerosol classification schemes (Burton *et al.*, 2012; Groß *et al.*, 2013b) were developed based on airborne HSRL measurements at 532 nm. It is an open question how the present classification schemes can be transferred to measurements with the ATLID system on EarthCARE at 355 nm. In this work, we present an analysis of the wavelength dependence of the lidar ratio $S_p$ and the particle linear depolarization ratio $\delta_p$, required for an aerosol classification with ATLID measurements, for five main aerosol types and aerosol mixtures of the Earth's atmosphere – mineral dust, mineral dust mixtures, marine aerosols, biomass burning mixtures and volcanic ash.

## 2. Methods

### 2.1. Data basis

In this study, we use data from five different field experiments: the Lindenberg Aerosol Characterization Experiment (LACE) (Ansmann *et al.*, 1998), the Saharan mineral dust experiments, SAMUM-1 (Heintzenberg, 2009) and SAMUM-2 (Ansmann *et al.*, 2011), the European integrated project on

**Table 1.** Mean values and mean systematic uncertainties for the intensive optical properties $S_p$ and $\delta_p$ of different aerosol types measured with WALES, MULIS and POLIS. Numbers in brackets give the number of measurements.

| Aerosol type | WALES 532 nm | MULIS 532 nm | POLIS 355 nm | Field experiment | Reference |
|---|---|---|---|---|---|
| $S_p$ (sr) | | | | | |
| Saharan dust | 48 ± 5 (4) | 56 ± 5[a] (13) | | SAMUM-1 | Esselborn *et al.* (2009); Tesche *et al.* (2009) |
| | | | 58 ± 8 (6) | SAMUM-2 | Groß *et al.* (2011a) |
| Dust mixture | 50 ± 4 (5) | | 54 ± 3 (6) | SAMUM-2 | Groß *et al.* (2011a, 2013b) |
| ABB mixture | 63 ± 7 (5) | 69 ± 8 (13) | 76 ± 12 (12) | SAMUM-2 | Groß *et al.* (2011a, 2013b) |
| CBB | 69 ± 17 (1) | | | LACE98 | Groß *et al.* (2013b) |
| Marine[b] | 18 ± 5 (5) | 18 ± 2 (2) | 18 ± 4 (4) | SAMUM-2 | Groß *et al.* (2011a, 2013b) |
| Anthropogenic | 56 ± 6 (4) | | | EUCAARI | Groß *et al.* (2013a) |
| Volcanic ash | | 50 ± 5 (2) | 55 ± 5 (2) | Eyjafjalla | Groß *et al.* (2012) |
| $\delta_p$ (%) | | | | | |
| Saharan dust | 32 ± 2 (4) | 32 ± 2 (18) | | SAMUM-1 | Esselborn *et al.* (2009); Freudenthaler *et al.* (2009) |
| | | | 25 ± 2 (6) | SAMUM-2 | Groß *et al.* (2011a) |
| Dust mixture | 27 ± 2 (5) | 24 ± 4 (5) | 17 ± 3 (6) | SAMUM-2 | Groß *et al.* (2011a, 2013b) |
| ABB mixture | 14 ± 2 (5) | 16 ± 1 (13) | 16 ± 3 (12) | SAMUM-2 | Groß *et al.* (2011a, 2013b) |
| CBB | 7 ± 2 (1) | | | LACE98 | Groß *et al.* (2013b) |
| Marine[b] | 3 ± 2 (5) | 2 ± 1 (2) | 2 ± 1 (4) | SAMUM-2 | Groß *et al.* (2011a, 2013b) |
| Anthropogenic | 6 ± 1 (4) | | | EUCAARI | Groß *et al.* (2013a) |
| Volcanic ash | | 37 ± 2 (2) | 35 ± 2 (2) | Eyjafjalla | Groß *et al.* (2012) |

ABB, African biomass burning; CBB, Canadian biomass burning.
[a]Coordinated ground-based measurements with the BERTHA system (Althausen *et al.*, 2000) of TROPOS, Leipzig, as no Raman lidar measurements were performed with MULIS during SAMUM-1. Both systems were located next to each other in a horizontally very homogeneous atmosphere.
[b]Relative humidity in the marine aerosol layer ≥50%.

Aerosol Cloud Climate and Air Quality Interactions (EUCAARI) (Kulmala *et al.*, 2009), and the Eyjafjalla volcanic ash measurements at Munich university (Groß *et al.*, 2012; Wiegner *et al.*, 2012). During these field experiments, aerosol properties have been studied by an extensive set of aerosol *in situ* instruments on board the DLR Falcon research aircraft by an airborne HSRL system measuring the lidar ratio and the particle depolarization ratio at 532 nm and by two ground-based polarization sensitive Raman lidar systems of the Ludwig-Maximilians-Universität (LMU), München, operational at 532 and 355 nm. For the volcanic ash measurements, no airborne HSRL measurements were performed. On the basis of this comprehensive dataset, we assess whether the aerosol classification scheme developed for 532 nm (Groß *et al.*, 2013b) is applicable to future EarthCARE lidar measurements at 355 nm. Although several studies on lidar derived aerosol optical properties have been performed, we restrict our comparisons to the above mentioned dataset to avoid uncertainties which might result from different instrument setups or combinations, or different calibration techniques. Furthermore, only few studies with simultaneously performed lidar measurements of the lidar ratio and the particle linear depolarization ratio at 355 and 532 nm together with *in situ* observations are reported in the literature so far. Discussions of the used dataset to former studies can be found in the references listed in Table 1. Information about the corresponding *in situ* measurements can be found in Groß *et al.* (2013b) and Weinzierl *et al.* (2011) and the references therein.

## 2.2. Lidar systems

In this section, we give a short overview of the lidar systems used to examine the wavelength dependence of $S_p$ and $\delta_p$ for different aerosol types. Details on instrument performance and measurement uncertainties are discussed in the corresponding references.

POLIS (Groß *et al.*, 2008) is a ground-based small portable lidar system developed and operated by the Meteorological Institute of the LMU. Measurements were either performed in the depolarization mode, measuring the cross- and co-polarized lidar return at 355 nm, or in the Raman mode measuring the elastically scattered signal return at 355 nm and the $N_2$-Raman shifted return at 387 nm.

MULIS (Freudenthaler *et al.*, 2009) is a ground-based mobile multi-wavelength lidar system developed and operated by the Meteorological Institute of the LMU. It provides measurements of the elastically backscattered signals at 355, 532 (co- and cross-polarized) and 1064 nm, and of the $N_2$-Raman shifted signals at 387 and 607 nm.

WALES (WAter vapor Lidar Experiment in Space) (Wirth *et al.*, 2009), developed and operated by the DLR, is primarily an airborne differential absorption lidar (DIAL) system for water vapor measurements within the absorption band at 935 nm whose primary objective was the preparation of a space borne mission mapping the global water vapor distribution. Additional polarization sensitive aerosol channels at 532 and 1064 nm and a high spectral resolution capacity at 532 nm (Esselborn *et al.*, 2008) enable simultaneous aerosol measurements.

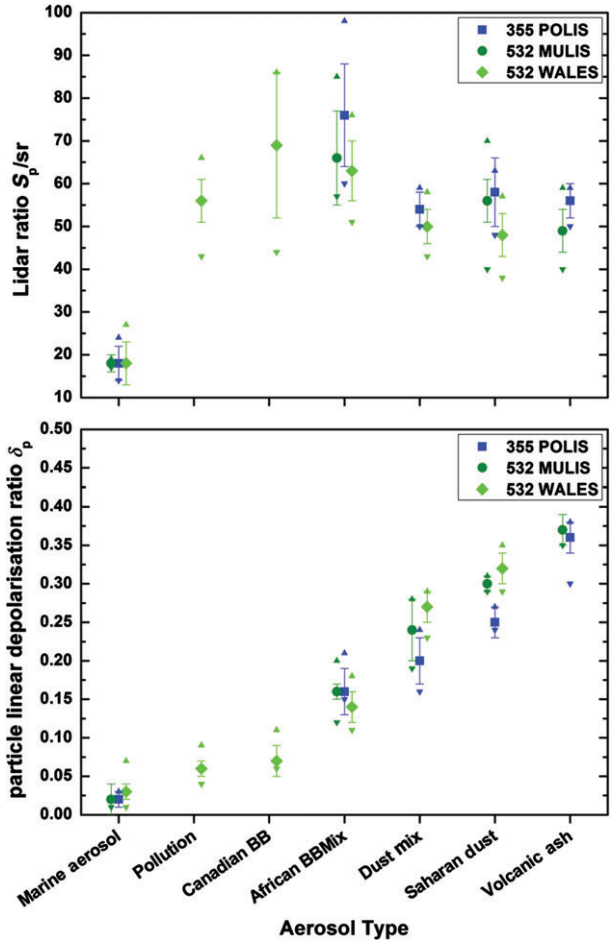


**Figure 1.** Lidar ratio (top panel) and particle linear depolarization ratio (bottom panel) of the mean values found for the different aerosol types at 355 and 532 nm from POLIS (355 nm), MULIS and WALES (both 532 nm) measurements. The error bars show the mean systematic uncertainties; the triangles show the maximum and minimum values.

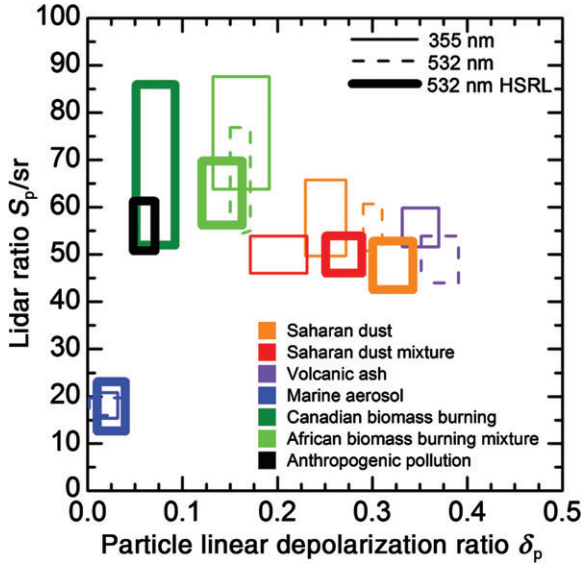


**Figure 2.** Aerosol lidar ratio versus particle linear depolarization ratio for various atmospheric aerosol types measured with the lidar systems POLIS at 355 nm, and MULIS and WALES at 532 nm. The rectangles denote the mean values plus/minus the mean uncertainties as summarized in Table 1.

## 3. Results and discussion

### 3.1. Wavelength dependence of optical properties

Figure 1 shows the mean values of the lidar ratio $S_p$ and the particle linear depolarization ratio $\delta_p$ for different aerosol types. The error bars indicate the mean systematic errors of these values. A general information about the error calculation of the different variables is given by Freudenthaler *et al.* (2009), Esselborn *et al.* (2008) and Groß *et al.* (2011b). The errors of the single measurements used for this work are discussed in corresponding references listed in Table 1. No wavelength dependency of the lidar ratio is visible for marine aerosol, Saharan mineral dust and dust mixtures (Figure 1, top panel). For volcanic ash and African biomass burning mixtures, the mean $S_p$ value at 355 nm is slightly higher than at 532 nm, but considering the measurement uncertainties this difference is not significant. In the bottom panel of Figure 1, the particle linear depolarization ratio $\delta_p$ is depicted for different aerosol types. No wavelength dependency for marine aerosol, African biomass burning mixtures and volcanic ash is observed. In contrast, we find significantly lower values of $\delta_p$ for Saharan dust at 355 nm, and consequently also for dust mixtures at which it has to be kept in mind that $\delta_p$ in dust mixtures dependents on the type and the amount of aerosol mixed with Saharan dust. In our case, we see a strong contribution of Saharan dust most probably mixed with marine aerosols, which is in good agreement to former findings (Mona *et al.*, 2006). As we do not have coordinated $S_p$ and $\delta_p$ measurements at 355 and 532 nm for pure biomass burning aerosol and anthropogenic pollution airmasses from the three used lidar systems, the wavelength dependency for these two aerosol types will not be discussed here.

Table 1 summarizes the main findings of this section for the different aerosol types. Besides the values for $S_p$ and $\delta_p$ also the measurement uncertainties and the corresponding references are summarized.

### 3.2. Classification scheme

In this section, we discuss the applicability of the previously (Burton *et al.*, 2012; Groß *et al.*, 2013b) developed aerosol classification scheme at 532 nm for EarthCARE measurements at 355 nm. Similar to Burton *et al.* (2012) and Groß *et al.* (2013b), the intensive lidar optical parameters ($S_p$ and $\delta_p$) are presented in a two-dimensional $S_p$–$\delta_p$ parameter space in Figure 2, which additionally shows the values for both wavelengths, 355 and 532 nm, in one plot.

The cluster for marine aerosol agrees well for the different wavelengths, confirming the applicability of the classification thresholds derived by Groß *et al.* (2013b) at 532 nm also for 355 nm. For volcanic ash and African biomass burning mixture the data clusters at both wavelengths overlap. However, the mean values and uncertainty ranges at both wavelengths differ.

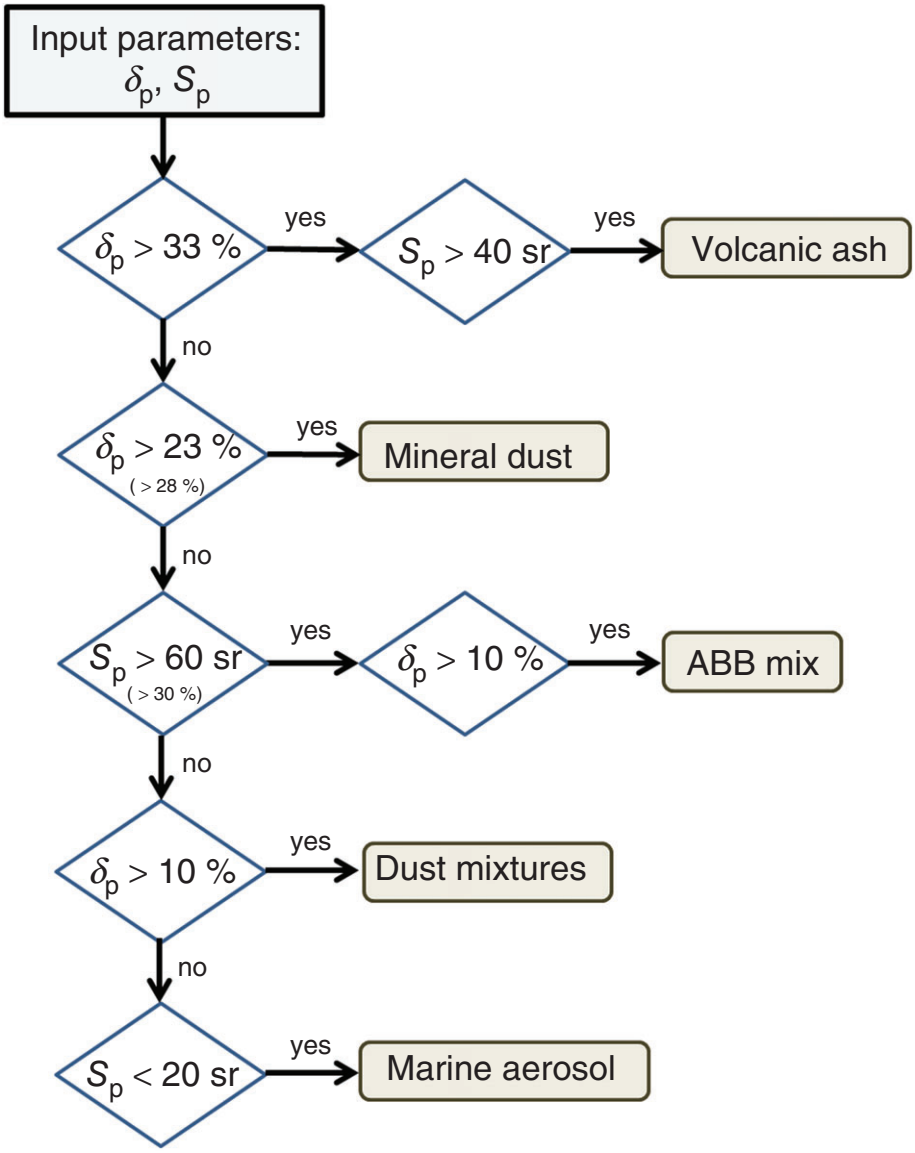


**Figure 3.** Schematic flowchart of the aerosol type classification based on lidar ratio $S_p$ and particle linear depolarization ratio $\delta_p$ information at 355 nm; values at 532 nm [adapted from Groß *et al.* (2013b)] are shown in brackets. ABB mix denotes African biomass burning mixtures.

For African biomass burning mixture the thresholds adapted by Groß *et al.* (2013b) retain ($S_p > 60$ sr and $\delta_p > 10$ %). For volcanic ash the thresholds for the aerosol classification scheme at 355 nm must be adapted to values higher 40 sr for $S_p$ and 33 % for $\delta_p$. The same holds for Saharan dust, were we do not see an overlap of the data clusters at all. The thresholds for the classification at 355 nm are 23% and 33% as lower and upper $\delta_p$ values, respectively, and 60 sr as upper threshold for $S_p$.

Figure 3 presents the adapted aerosol type classification thresholds for lidar measurements (e.g. by ATLID on EarthCARE) at 355 nm on the basis of the results of this study. Using this classification scheme, it has to be kept in mind that some aerosol types show only small differences in the lidar optical properties (see Figures 1 and 2) and therefore they are harder to distinguish than other aerosol types. In addition, highly accurate lidar measurements with small uncertainties are necessary for correct aerosol type classification.

### 3.3. Discussion

The optical properties of aerosols are correlated with the aerosols microphysical properties like particle size, particle shape and chemical composition (Gasteiger *et al.*, 2011). During short- to long-range transport, the microphysical properties can be modified by various mechanisms (Weinzierl *et al.*, 2011), and with that the optical properties and the measurement values of $S_p$ and $\delta_p$ and their wavelength dependency can be influenced. For example, Amiridis *et al.* (2009) found from regular Raman lidar measurements that the values and wavelength dependence of the lidar ratio for biomass burning aerosols may change with time since emission. This may be caused by changing of the microphysical properties during transport. Another

indication for the modification of optical properties during transport was found for mineral dust: during a strong Saharan dust outbreak in 2008 dual-wavelength depolarization measurements were performed over Central Europe (Wiegner *et al.*, 2011). High $\delta_p$ values of 30% were found at 355 nm compared to values of 25% during SAMUM-2. However, the measurements by Wiegner *et al.* (2011) cover only one case, and in addition, the dust load was very low resulting in large measurement uncertainties preventing a clear conclusion. More measurements of $S_p$ and $\delta_p$ in mineral dust plumes at different age after emission are necessary to draw final conclusions on changes of $S_p$ and $\delta_p$ as a result of aging processes.

Measurements of fresh and aged aerosol plumes, in particular of biomass burning aerosols and mineral dust, at different wavelengths are therefore crucial. Furthermore the aerosol classification scheme at 355 nm has to be extended for further basic aerosol types like anthropogenic pollution and cirrus clouds.

## 4. Conclusion

We presented a comparison of a comprehensive dataset of coordinated measurements with polarization sensitive Raman and HSRL lidar systems at 355 and 532 nm and examined the wavelength dependency of the lidar optical aerosol parameters, $S_p$ and $\delta_p$. On the basis of our analysis, we adapted the thresholds of the already existing aerosol classification scheme at 532 nm so that this classification scheme is applicable for future satellite lidar observations at 355 nm on board EarthCARE. Our study shows that for some aerosol types (e.g. marine aerosol) the classification thresholds found for 532 nm are also applicable at 355 nm. For other aerosol types (e.g. mineral dust), the classification values have to be adapted for 355 nm.

We see this study only as a starting point for an aerosol classification scheme at 355 nm. Currently the dataset to develop a comprehensive classification scheme for global satellite lidar measurements at 355 nm is limited, especially with respect to different measurement locations and to aerosol mixtures. Thus questions concerning the influence of aerosol aging, natural variability, and complex aerosol mixtures on a global classification scheme cannot be answered yet. Future research activities are crucial to extend the database for aerosol type classification at 355 nm. Especially, more measurements of basic aerosol types such as anthropogenic pollution or fresh biomass burning aerosol are necessary. In addition, special attention should be paid to the investigation of the effect of aerosol aging processes on the lidar optical parameters $S_p$ and $\delta_p$ at 355 nm. Such investigations may result in different classification thresholds for fresh and aged aerosols of the same type. The Saharan Aerosol Long-Range TRansport and Aerosol Cloud interaction experiment (SALTRACE: http://www.pa.op.dlr.de/saltrace/) performed in June/July 2013 in the Caribbean may help to answer some of the aging-related questions. Furthermore, model calculations using complex particle shapes and *in situ* measurements as input parameters are helpful to study the sensitivity of the lidar optical properties $S_p$ and $\delta_p$ on the different microphysical properties.

### Acknowledgements

This work has been funded partly by the HALO-SPP (No. 1294/2) under contract Nr. KI1567/1-1, and by the Helmholtz Association (VH-NG-606, Helmholtz-Hochschul-Nachwuchsforschergruppe AerCARE).

## References

Althausen D, Mueller D, Ansmann A, Wandinger U, Hube H, Clauder E, Zoerner S. 2000. Scanning six-wavelength eleven-channel aerosol lidar. *Journal of Atmospheric and Oceanic Technology* **17**: 1469–1482.

Amiridis V, Balis DS, Giannakaki E, Stohl A, Kazadzis S, Koukouli ME, Zanis P. 2009. Optical characteristics of biomass burning aerosols over southeastern Europe determined from UV-Raman lidar measurements. *Atmospheric Chemistry and Physics* **9**(7): 2431–2440, doi: 10.5194/acp-9-2431-2009.

Ansmann A, Wandinger U, Riebesell M, Weitkamp C, Michaelis W. 1992. Independent measurement of extinction and backscatter profiles in cirrus clouds by using a combined Raman elastic-backscatter lidar. *Applied Optics* **31**(33): 7113–7131, doi: 10.1364/AO.31.007113.

Ansmann A, Wandinger U, Wiedensohler A, Leiterer U. 1998. Lindenberg aerosol characterization experiment 1998 (lace 98): overview. *Journal of Geophysical Research* **107**(21): 8129, doi: 10.1029/2000JD000233.

Ansmann A, Petzold A, Kandler K, Tegen I, Wendisch M, Mueller D, Weinzierl B, Mueller T, Heintzenberg J. 2011. Saharan mineral dust experiments SAMUM1 and SAMUM2: what have we learned? *Tellus B* **63**(4): 403–429, doi: 10.1111/j.1600-0889.2011.00555.x.

Bond TC, Doherty SJ, Fahey DW, Forster PM, Berntsen T, DeAngelo BJ, Flanner MG, Ghan S, Käarcher B, Koch D, Kinne S, Kondo Y, Quinn PK, Sarofim MC, Schultz MG, Schulz M, Venkataraman C, Zhang H, Zhang S, Bellouin N, Guttikunda SK, Hopke PK, Jacobson MZ, Kaiser JW, Klimont Z, Lohmann U, Schwarz JP, Shindell D, Storelvmo T, Warren SG, Zender CS. 2013. Bounding the role of black carbon in the climate system: a scientific assessment. *Journal of Geophysical Research: Atmospheres* **118**(11): 5380–5552, doi: 10.1002/jgrd.50171.

Burton SP, Ferrare RA, Hostetler CA, Hair JW, Rogers RR, Obland MD, Butler CF, Cook AL, Harper DB, Froyd KD. 2012. Aerosol classification using airborne high spectral resolution lidar measurements methodology and examples. *Atmospheric Measurement Techniques* **5**(1): 73–98, doi: 10.5194/amt-5-73-2012.

Burton SP, Ferrare RA, Vaughan MA, Omar AH, Rogers RR, Hostetler CA, Hair JW. 2013. Aerosol classification from airborne HSRL and comparisons with the CALIPSO vertical feature mask. *Atmospheric Measurement Techniques* **6**(5): 1397–1412, doi: 10.5194/amt-6-1397-2013.

Esselborn M, Wirth M, Fix A, Tesche M, Ehret G. 2008. Airborne high spectral resolution lidar for measuring aerosol extinction and backscatter coefficients. *Applied Optics* **47**(3): 346–358, doi: 10.1364/AO.47.000346.

Esselborn M, Wirth M, Fix A, Weinzierl B, Rasp K, Tesche M, Petzold A. 2009. Spatial distribution and optical properties of Saharan dust observed by airborne high spectral resolution lidar during SAMUM 2006. *Tellus B* **61**(1): 131–143, doi: 10.1111/j.1600-0889.2008.00394.x.

Forster P, Ramaswamy V, Artaxo P, Berntsen T, Betts R, Fahey DW, Haywood J, Lean J, Lowe DC, Myhre G, Nganga J, Prinn R, Raga G, Schulz M, Van Dorland R. 2007. Changes in atmospheric constituents

and in radiative forcing. In *Climate Change 2007: The Physical Science Basis. Contribution of Working Group I to the Fourth Assessment Report of the Intergovernmental Panel on Climate Change*, Solomon S, Qin D, Manning M, Chen Z, Marquis M, Averyt KB, Tignor M, Miller HL (eds). Cambridge University Press: Cambridge, UK and New York, NY.

Freudenthaler V, Esselborn M, Wiegner M, Heese B, Tesche M, Ansmann A, Müller D, Althausen D, Wirth M, Fix A, Ehret G, Knippertz P, Toledano C, Gasteiger J, Garhammar M, Seefeldner M. 2009. Depolarization ratio profiling at several wavelengths in pure Saharan dust during SAMUM 2006. *Tellus B* **61**(1): 165–179, doi: 10.1111/j.1600-0889.2008.00396.x.

Gasteiger J, Wiegner M, Groß S, Freudenthaler C, Toledano V, Tesche M, Kandler K. 2011. Modeling lidar-relevant optical properties of complex mineral dust aerosols. *Tellus B* **63**: 725–741, doi: 10.1111/j.1600-0889.2011.00559.x.

Groß S, Freudenthaler V, Toledano C, Seefeldner M, Wiegner M. 2008. Mini-lidar measurements of particle depolarization and Raman scattering of Saharan-dust and biomass burning at 355 nm during SAMUM 2. In Proceedings of 24th International Laser Radar Conference, Boulder, CO, 23–27 June 2008. S04P-10.

Groß S, Tesche M, Freudenthaler V, Toledano C, Wiegner M, Ansmann A, Althausen D, Seefeldner M. 2011a. Characterization of Saharan dust, marine aerosols and mixtures of biomass burning aerosols and dust by means of multi-wavelength depolarization- and Raman-measurements during SAMUM-2. *Tellus B* **63**(4): 706–724, doi: 10.1111/j.1600-0889.2011.00556.x.

Groß S, Wiegner M, Freudenthaler V, Toledano C. 2011b. Lidar ratio of Saharan dust over Cape Verde Islands: assessment and error calculation. *Journal of Geophysical Research* **116**: D15203, doi: 10.1029/2010JD015435.

Groß S, Freudenthaler V, Wiegner M, Gasteiger J, Geiß A, Schnell F. 2012. Dual wavelength linear depolarization ratio of volcanic aerosols: lidar measurements of the Eyjafjallajkull plume over Maisach, Germany. *Atmospheric Environment* **48**: 85–96, doi: 10.1016/j.atmosenv.2011.06.017.

Groß S, Esselborn M, Abicht F, Wirth M, Fix A, Minikin A. 2013a. Airborne high spectral resolution lidar observation of pollution aerosol during EUCAARI-Longrex. *Atmospheric Chemistry and Physics* **13**(5): 2435–2444, doi: 10.5194/acp-13-2435-2013.

Groß S, Esselborn M, Weinzierl B, Wirth M, Fix A, Petzold A. 2013b. Aerosol classification by airborne high spectral resolution lidar observations. *Atmospheric Chemistry and Physics* **13**(5): 2487–2505, doi: 10.5194/acp-13-2487-2013.

Heintzenberg J. 2009. The SAMUM-1 experiment over southern Morocco: overview and introduction. *Tellus B* **61**(1): 2–11, doi: 10.1111/j.1600-0889.2008.00403.x.

Kacenelenbogen M, Vaughan MA, Redemann J, Hoff RM, Rogers RR, Ferrare RA, Russell PB, Hostetler CA, Hair JW, Holben BN. 2011. An accuracy assessment of the CALIOP/CALIPSO version 2/version3 daytime aerosol extinction product based on a detailed multi-sensor, multi-platform case study. *Atmospheric Chemistry and Physics* **11**(8): 3981–4000, doi: 10.5194/acp-11-3981-2011.

Kulmala M, Asmi A, Lappalainen HK, Carslaw KS, Pöschl U, Baltensperger U, Hov Ø, Brenquier J-L, Pandis SN, Facchini MC, Hansson H-C, Wiedensohler A, O'Dowd CD. 2009. Introduction: European integrated project on aerosol cloud climate and air quality interactions (EUCAARI) integrating aerosol research from nano to global scales. *Atmospheric Chemistry and Physics* **9**(8): 2825–2841, doi: 10.5194/acp-9-2825-2009.

Mona L, Amodeo A, Pandolfi M, Pappalardo G. 2006. Saharan dust intrusions in the Mediterranean area: three years of Raman lidar measurements. *Journal of Geophysical Research* **111**: D16203, doi: 10.1029/2005JD006569.

Omar AH, Winker DM, Vaughan MA, Hu Y, Trepte CR, Ferrare RA, Lee K-P, Hostetler CA, Kittaka C, Rogers RR, Kuehn RE, Liu Z. 2009. The CALIPSO automated aerosol classification and lidar ratio selection algorithm. *Journal of Atmospheric and Oceanic Technology* **26**: 1994–2014.

Penner JE, Andreae M, Annegarn H, Barrie L, Feichter J, Hegg D, Jayaraman A, Leaitch R, Murphy D, Nganga J, Pitari G. 2001. *Climate Change 2001: The Scientific Assessment*. Cambridge University Press: New York, NY, 289–348.

Penner JE, Xu L, Wang M. 2011. Satellite methods underestimate indirect climate forcing by aerosols. *Proceedings of the National Academy of Sciences* **108**(33): 13404–13408, doi: 10.1073/pnas.1018526108.

Piironen P, Eloranta EW. 1994. Demonstration of a high-spectral-resolution lidar based on an iodine absorption filter. *Optics Letters* **19**(3): 234–236, doi: 10.1364/OL.19.000234.

Tesche M, Ansmann A, Müller D, Althausen D, Mattis I, Heese B, Freudenthaler V, Wiegner M, Esselborn M, Pisani G, Knippertz P. 2009. Vertical profiling of Saharan dust with Raman lidars and airborne HSRL in southern morocco during SAMUM. *Tellus B* **61**(1): 144–164, doi: 10.1111/j.1600-0889.2008.00390.x.

Weinzierl B, Sauer D, Esselborn M, Petzold A, Veira A, Rose M, Mund S, Wirth M, Ansmann A, Tesche M, Gross S, Freudenthaler V. 2011. Microphysical and optical properties of dust and tropical biomass burning aerosol layers in the Cape Verde region an overview of the airborne in situ and lidar measurements during SAMUM-2. *Tellus B* **63**(4): 589–618, doi: 10.1111/j.1600-0889.2011.00566.x.

Wiegner M, Groß S, Freudenthaler V, Schnell F, Gasteiger J. 2011. The May/June 2008 Saharan dust event over Munich: intensive aerosol parameters from lidar measurements. *Journal of Geophysical Research* **116**(D23): 213, doi: 10.1029/2011JD016619.

Wiegner M, Gasteiger J, Groß S, Schnell F, Freudenthaler V, Forkel R. 2012. Characterization of the Eyjafjallajkull ash-plume: potential of lidar remote sensing. *Physics and Chemistry of the Earth* Parts A/B/C **45–46**: 79–86, doi: 10.1016/j.pce.2011.01.006.

Winker DM, Hunt WH, McGill MJ. 2007. Initial performance assessment of CALIOP. *Geophysical Research Letters* **34**: L19803.

Wirth M, Fix A, Mahnke P, Schwarzer H, Schrandt F, Ehret G. 2009. The airborne multi-wavelength H2O-DIAL WALES: system design and performance. *Applied Physics B: Lasers and Optics* **96**(1): 201–213, doi: 10.1007/s00340-009-3365-7.